NeuroImage: Clinical 28 (2020) 102386

Contents lists available at ScienceDirect

NeuroImage: Clinical

journal homepage: www.elsevier.com/locate/ynicl

Image reconstruction methods affect software-aided assessment of pathologies of [^{18}F]flutemetamol and [^{18}F]FDG brain-PET examinations in patients with neurodegenerative diseases

Elin Lindström[a,b,*], Jenny Oddstig[c], Torsten Danfors[a], Jonas Jögi[d], Oskar Hansson[e,f], Mark Lubberink[a,b]

[a] Nuclear Medicine and PET, Department of Surgical Sciences, Uppsala University, SE-751 85 Uppsala, Sweden
[b] Medical Physics, Uppsala University Hospital, SE-751 85 Uppsala, Sweden
[c] Radiation Physics, Skåne University Hospital, SE-221 85 Lund, Sweden
[d] Clinical Physiology and Nuclear Medicine, Skåne University Hospital, SE-221 85 Lund, Sweden
[e] Clinical Memory Research Unit, Lund University, SE-221 00 Lund, Sweden
[f] Memory Clinic, Skåne University Hospital, SE-205 02 Malmö, Sweden

ARTICLE INFO

Keywords:
[^{18}F]Flutemetamol
[^{18}F]FDG
Software-aided diagnosis
Quantification
PET imaging
PET image reconstruction

ABSTRACT

Purpose: To assess how some of the new developments in brain positron emission tomography (PET) image reconstruction affect quantitative measures and software-aided assessment of pathology in patients with neurodegenerative diseases.

Methods: PET data were grouped into four cohorts: prodromal Alzheimer's disease patients and controls receiving [^{18}F]flutemetamol, and neurodegenerative disease patients and controls receiving [^{18}F]FDG PET scans. Reconstructed images were obtained by ordered-subsets expectation maximization (OSEM; 3 iterations (i), 16/34 subsets (s), 3/5-mm filter, ± time-of-flight (TOF), ± point-spread function (PSF)) and block-sequential regularized expectation maximization (BSREM; TOF, PSF, β-value 75–300). Standardized uptake value ratios (SUVR) and z-scores were calculated (CortexID Suite, GE Healthcare) using cerebellar gray matter, pons, whole cerebellum and whole brain as reference regions.

Results: In controls, comparable results to the normal database were obtained with OSEM 3i/16 s 5-mm reconstruction. TOF, PSF and BSREM either increased or decreased the relative uptake difference to the normal subjects' database within the software, depending on the tracer and chosen reference area, i.e. resulting in increased absolute z-scores. Normalizing to pons and whole brain for [^{18}F]flutemetamol and [^{18}F]FDG, respectively, increased absolute differences between reconstructions methods compared to normalizing to cerebellar gray matter and whole cerebellum when applying TOF, PSF and BSREM.

Conclusions: Software-aided assessment of patient pathologies should be used with caution when employing other image reconstruction methods than those used for acquisition of the normal database.

1. Introduction

Positron emission tomography (PET) imaging of patients with suspected neurodegenerative disease can reveal pathological changes at an early stage. However, differential diagnosis between disorders can be difficult and reliable assessment of brain-PET images therefore requires a high level of expertise and experience. Computer-based tools for image analysis are an important part of clinical evaluation of examinations and may assist with objective clinical interpretation and provide support in the diagnosis of neurodegenerative diseases. Several software-aided diagnosis systems for neuroimaging are available, e.g. Brass (Hermes Medical Solutions), CortexID Suite (GE Healthcare), NeuroQ (Syntermed), Syngo.PET (Siemens), MiM Neuro (MIM), and Amyloid analyser (Fraunhofer-Mevis). CortexID, used in the present study, is a fully automated tool for analysis and quantification of [^{18}F]FDG and β-amyloid brain PET examinations, and includes standardized uptake value ratio (SUVR) reference databases generated from healthy volunteer data. In addition, most of these software applications provide 3D-stereotactic surface projection (SSP) maps which have improved the accuracy and sensitivity of decision-making and thereby support a

* Corresponding author at: Nuclear medicine and PET, Department of Surgical Sciences, Uppsala University, SE-751 85 Uppsala, Sweden.
E-mail address: elin.lindstrom@surgsci.uu.se (E. Lindström).

https://doi.org/10.1016/j.nicl.2020.102386
Received 29 January 2020; Received in revised form 28 July 2020; Accepted 17 August 2020
Available online 19 August 2020

better clinical care of patients with neurodegenerative diseases (Minoshima et al., 1995; Ishii et al., 2006; Drzezga, 2009; Partovi et al., 2017).

New developments in PET instrumentation and software design, such as time-of-flight (TOF) capable PET/computer tomography (CT) scanners, integrated point-spread function (PSF) recovery and regularized reconstruction methods have all resulted in improved image signal-to-noise ratio. Regularized image reconstruction allows for fully convergent iterative reconstruction of PET data, which, in contrast to conventional non-regularized methods, results in less noise and better recovery of radioactivity concentration. The commercially available block-sequential regularized expectation maximization (BSREM) (Q.Clear; GE Healthcare) reconstruction method implements regularization by a relative difference penalty (De Pierro and Yamagishi, 2001; Nuyts et al., 2002; Ross, 2014), and allows the user to adjust the strength of the activity-dependent smoothing. Studies addressing whole body [^{18}F]FDG on various PET/CT scanners have shown for BSREM to reduce image noise without impeding the tumor detectability, or vice versa, to improve tumor detectability at similar noise levels as ordered-subsets expectation maximization (OSEM) (Teoh et al., 2016; Sah et al., 2017; Lindström et al., 2018; Trägårdh et al., 2019; Björsdorff et al., 2019). Other studies have also shown the need to adjust the setting of β depending on the tracer and application being used (Lindström et al., 2019, 2020).

To our knowledge, the effect of regularized reconstruction on brain-PET images has not yet been described. The reference databases in the software-aided diagnosis systems referred above have often been acquired several years ago and over a long time period, using scanners and image reconstruction methods that provided poorer image quality and lower image resolution than the current state of the art systems using higher sensitivity scanners, TOF, PSF recovery and regularized reconstruction.

The aim of the present study was to evaluate how some of the improved PET image reconstructions affect quantitative measures and assessment of patients with neurodegenerative diseases using dedicated software.

2. Material and methods

2.1. Subjects

PET data were grouped into four cohorts: 16 patients with clinically-diagnosed prodromal Alzheimer's disease (AD) with Aβ pathology (abnormal cerebrospinal fluid Aβ42/Aβ40 ratio) (Janelidze et al., 2017) and a control cohort comprising 20 healthy volunteers without Aβ pathology (normal cerebrospinal fluid Aβ42/Aβ40 ratio) underwent [^{18}F]flutemetamol PET scans, and 20 patients referred for dementia evaluation and a control cohort comprising 13 melanoma patients without brain involvement underwent [^{18}F]FDG PET. Due to a regional z-score inclusion criteria of −2 or less for the [^{18}F]FDG patient cohort (see further details under 2.3 Quantification) only 12 patients out of 20 were included in the analysis. Cohort characteristics are presented in Tables 1 and 2. This study was a dual-center collaboration and the recruitment and examination took place at Skåne University Hospital ([^{18}F]flutemetamol) in Malmö and Lund, Sweden and at Uppsala University Hospital ([^{18}F]FDG) in Uppsala, Sweden, while the analyses of PET images were performed in Uppsala. The [^{18}F]flutemetamol patients were included in the Swedish BioFINDER 2 study and [^{18}F]FDG patients were clinical routine examinations. All scans were acquired between 2016 and 2018. Study approvals were obtained from the regional ethical authorities of the participating centers (Malmö/Lund reference number 2016/1053, Uppsala reference number 2019/00092).

2.2. Imaging

All subjects were scanned on a 4-ring Discovery MI digital TOF PET/CT scanner (GE Healthcare, Marlborough, MA, USA) (Hsu et al., 2017). [^{18}F]Flutemetamol PET images (patients and healthy volunteers) were acquired as a 20-min static scan starting approximately 90 min after injection of 185 MBq (2.4 ± 0.5, range 1.5–3.3 MBq/kg) of [^{18}F]flutemetamol. Neurodegenerative disease patients underwent a 10-min static scan starting approximately 45 min after injection of 3.2 ± 0.5 (range 2.2–4.4) MBq/kg of [^{18}F]FDG, while the control cohort of melanoma patients underwent a whole-body scan; for the present study the 2-min static scan of the brain bed position starting approximately 90 min after injection of 3.7 ± 0.4 (range 2.9–4.4) MBq/kg of [^{18}F]FDG was used. The PET image data were reconstructed by OSEM (± TOF, ± PSF, 3 iterations (i), 16/34 subsets (s), and 3/5 mm Gaussian post processing filter) and BSREM (always including TOF and PSF; β 75, 150, 225, and 300), applying all appropriate corrections i.e. the data were normalized and corrected for deadtime, random coincidences, scatter, and attenuation based on CT. A transaxial field of view of 250 mm and a 256 × 256 matrix resulted in 0.98 × 0.98 × 2.79 mm^3 voxels.

Table 1
Patient and control cohorts' characteristics.

	[^{18}F] Flutemetamol		[^{18}F] FDG	
Variable	**Patients**	**Controls**	**Patients**	**Controls**
Subjects n	16	20	12	13
Age mean ± SD	75 ± 5	59 ± 14	69 ± 9	58 ± 14
Gender	F:62.5% M:37.5%	F:45% M:55%	F:50% M:50%	F:62% M:38%
Scan duration [min]	20	20	10	2
Injected activity [MBq/kg]	2.6 ± 0.5 (1.9–3.2)*	2.3 ± 0.5 (1.5–3.3)*	3.2 ± 0.5 (2.2–4.4)	3.7 ± 0.4 (2.9–4.4)
Uptake time [min]	90	90	45	90

SD: standard deviation; F: female; M: male.
* Injected activity was 185 MBq.

Table 2
Diagnosis of [^{18}F]FDG neurodegenerative disease patients (n = 12).

Subject	Clinical diagnosis
1	AD + vascular PD
2	CBD
3	FTD
4	AD
5	CBD
6	FTD
7	AD
8	DLB
9	FTD
10	Vascular PD
11	FTD
12	AD

AD: Alzheimer's disease; PD: Parkinson's disease; CBD: cortical basal degeneration; FTD: frontotemporal dementia; DLB: dementia with Lewy bodies.AD: Alzheimer's disease; PD: Parkinson's disease; CBD: cortical basal degeneration; FTD: frontotemporal dementia; DLB: dementia with Lewy bodies.

2.3. Quantification

[^{18}F]Flutemetamol and [^{18}F]FDG activity were quantified using a fully automated post processing application, CortexID Suite 2.1 Ext. 6 (GE Healthcare, Marlborough, MA, USA). Each set of study data were compared to a dataset of normal controls provided through the software, with age-matched comparisons for [^{18}F]FDG. Semiquantitative

outcome measures were regional SUVR, calculated relative to a reference region, and z-scores. The reference regions were either pons or cerebellar gray matter for analysis of [^{18}F]flutemetamol examinations, and either whole cerebellum or whole brain for [^{18}F]FDG examinations. Z-scores define the number of standard deviations (σ) from the normal mean (μ), and are computed as follows,

$$z = \frac{x - \mu_{normal}}{\sigma_{normal}}. \quad (1)$$

where x is the individual value of the current examination. A positive z-score represents increased uptake relative to the normal reference data and, vice versa, a negative z-score represents reduced uptake. For clinical interpretation, regions with a resulting z-score equal to or higher than 2 is considered pathologic when assessing [^{18}F]flutemetamol examinations. Whereas a z-score equal to or lower than −2 is considered pathologic when assessing [^{18}F]FDG examinations.

For [^{18}F]flutemetamol, the evaluation was restricted to a composite region. For [^{18}F]FDG, a combination of prefrontal, precuneus and parietal regions was analyzed including both left and right regions. In the [^{18}F]FDG control cohort, all those regions were included in the analysis, while in the [^{18}F]FDG patient cohort, regions were included in the analysis given that the region had a z-score less than −2 for an OSEM reconstruction with 3 iterations, 16 subsets and 5 mm filter (3i/16s 5 mm) using whole cerebellum as reference. The composite region of all subjects in the [^{18}F]flutemetamol patient cohort were included in the analysis regardless of z-score value.

2.4. Graphics and statistical analysis

GraphPad Prism 8.3.0 and Matlab 2016b were used for graphics and statistical analysis. Non-parametric *t*-test (paired two tailed Wilcoxon's signed rank test) was applied with statistical difference of SUVR and z-score between reconstruction methods for $P < 0.05$. A post-hoc analysis was performed using the nonparametric Friedman test correcting for multiple comparisons using Dunn's statistical hypothesis testing, yielding adjusted P-values with family wise significance at 0.05. Cohen's d was computed for patients versus controls for each reconstruction method, and for each reconstruction method versus the reconstruction method that best matched the normal database.

3. Results

The control cohorts of both [^{18}F]flutemetamol and [^{18}F]FDG yielded comparable results to the normal database when using OSEM 3i/16s 5-mm reconstruction, without TOF and PSF, considering mean z-score. TOF, PSF modelling and BSREM either increased or decreased the relative uptake difference to the normal subjects' database within the CortexID software, depending on the tracer and chosen reference area, i.e. resulting in increased absolute z-scores. The patient cohorts of both [^{18}F]flutemetamol and [^{18}F]FDG followed similar trends as for the control cohorts.

3.1. [^{18}F]Flutemetamol

Example images are shown in Fig. 1 a and Fig. 2 a. SUVR and z-scores of the patient and control cohorts are shown in Figs. 3 and 4 with cerebellar gray matter and pons used as reference regions, respectively. Results of statistical tests with corrections for multiple comparisons are presented in heat maps (Fig. 5) and in more detail in the appendix (Table A.1).

In general, there were no significant differences in SUVR and z-score compared to OSEM 3i/16s 5 mm for the patient cohort with cerebellar gray matter used as reference (Figs. 3 and 5). For the control cohort, however, PSF reconstruction resulted in significantly lower SUVR and z-score compared to OSEM 3i/16s 5 mm with cerebellar gray matter used as reference (Figs. 3, 5, and 6). Meanwhile, all reconstructions with PSF and/or with a 3-mm filter, with the exception of OSEM 3i/16s 3 mm, resulted in significantly lower SUVR and z-score compared to OSEM 3i/16s 5 mm in both cohorts with pons used as reference (Figs. 4, 5, and 6).

3.1.1. Effect sizes

Cohen's d for [^{18}F]flutemetamol was similar regardless of reconstruction method and reference region, except for a small negative trend in Cohen's d found with additional reconstruction features when comparing patients to OSEM controls with pons as reference (Fig. 7).

3.2. [^{18}F]FDG

Example images are shown in Fig. 1 b and Fig. 2 b. SUVR and z-scores of the patient and control cohorts are shown in Figs. 8 and 9 with whole cerebellum and whole brain used as reference regions, respectively. Results of statistical tests with corrections for multiple comparisons are presented in heat maps (Fig. 10) and in more detail in the appendix (Table A.1). Notably, TOF, PSF and BSREM resulted in increased mean SUVR and z-score compared with OSEM with whole cerebellum as reference, while the same reconstruction features resulted in decreased mean SUVR and z-score compared to OSEM with whole brain as reference (Figs. 8, 9, and 11). In general, PSF reconstruction resulted in significantly higher SUVR and z-score compared to OSEM 3i/16s 5 mm, when whole cerebellum was used as reference (Fig. 10). Meanwhile, PSF reconstruction as well as reconstruction with TOF and 3 mm filter resulted in significantly lower SUVR and z-score compared to OSEM 3i/16s 5 mm with whole brain as reference (Fig. 10).

3.2.1. Effect sizes

Cohen's d for [^{18}F]FDG was roughly similar for all reconstructions when whole cerebellum was used as reference, regardless if comparisons were made to OSEM or the same reconstruction method (Fig. 12 a, b). A larger variation in Cohen's d for [^{18}F]FDG was found with whole brain as reference (Fig. 12 c, d).

4. Discussion

The aim of the present work was to evaluate how some of the novel and improved PET image reconstructions, such as including TOF, PSF modelling and regularized reconstruction, affect quantitative measures and assessments of patients with neurodegenerative diseases using dedicated software. The choice of reconstruction method and setting was found to affect the magnitude of SUVR and z-score levels when utilizing a software-aided diagnosis for assessing and comparing examinations to a normal reference database.

Employing improved PET image reconstruction methods increased the risk of false-positive and false-negative outcome measures, as the z-score gradually either dropped or increased depending on the tracer and chosen reference region. Various studies choose different reference regions (Mosconi et al., 2008; Josephs et al., 2012; Thurfjell et al., 2014; Joshi et al., 2015; Finnsson et al., 2019). In our study, four reference regions were considered for retrieving SUVR measures, two for each tracer. The choice of reference region will always affect the magnitude of SUVR levels, depending on the level of uptake in that specific area. The pons, for example, is a hot region in flutemetamol scans with a higher uptake than cerebellar gray matter resulting in lower SUVR measures when used as reference region.

For the present study, images were initially reconstructed using 16 different reconstruction methods. The highlighted reconstruction methods in the figures were representative of the entire dataset ranging from the basic method of OSEM 3i/16s 5 mm, which most closely reflected the database of the CortexID software, to the addition of TOF, PSF and lastly BSREM β150 that resulted in the largest difference to the database and standard OSEM reconstruction.

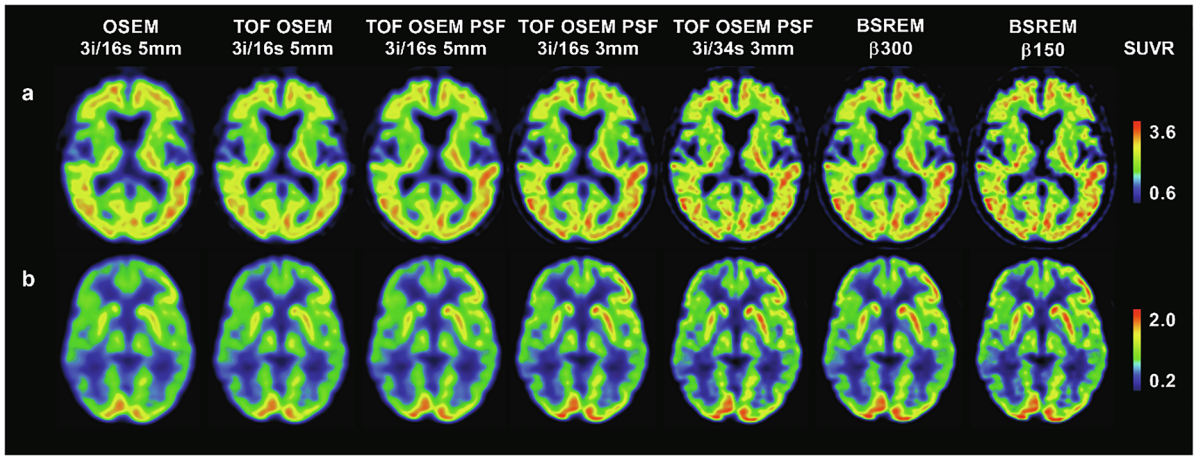

Fig. 1. SUVR images of two Alzheimer's disease patients PET examinations with [^{18}F]flutemetamol (a) and [^{18}F]FDG (b) using cerebellar gray matter and whole cerebellum as reference regions, respectively, for various reconstruction methods.

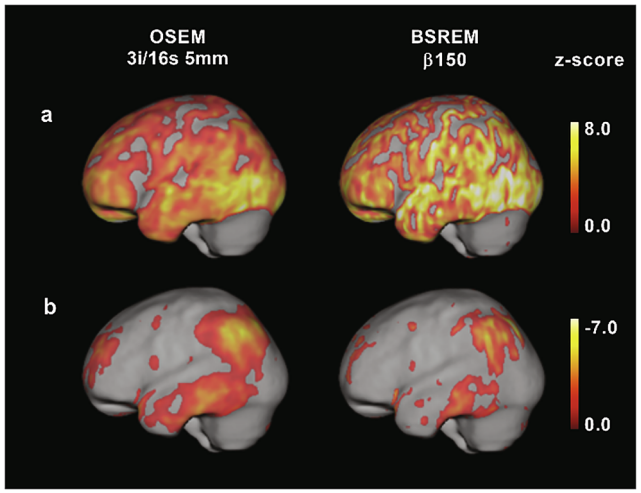

Fig. 2. 3D-SSP z-score images of two Alzheimer's disease patients (same as in Fig. 1) overlaid on MR template, [^{18}F]flutemetamol (a) and [^{18}F]FDG (b) using cerebellar gray matter and whole cerebellum as reference regions, respectively.

CortexID produced results for 20 and 26 different regions for [^{18}F]flutemetamol and [^{18}F]FDG, respectively, although not all of them were presented here. The composite region has previously been shown to adequately reflect changes in amyloid binding between Alzheimer's disease patient groups and healthy controls (Thurfjell et al., 2014). For [^{18}F]FDG, there is no such composite region available, hence we chose to analyze frontotemporal, precuneus and parietal regions instead. Additionally, due to the diversity of the [^{18}F]FDG patient cohort, regions that were not confirmed pathologic (z-score < -2) with cerebellum as reference in the OSEM 3i/16s 5 mm reconstruction were excluded from the analysis. Neurodegenerative diseases have certain distinguishable uptake patterns with higher uptake in varying regions causing mean SUVR measures over the entire cohort in our study to drop. However, the [^{18}F]FDG patient cohort resulted in similar trends as for the control cohort when compared to the normal database within the CortexID software. The effect of the different acquisition approaches between the [^{18}F]FDG patient and control cohort should also be minimal as it has previously been shown that z-scores were not affected by a low versus a normal dose of injected [^{18}F]FDG (Fällmar et al., 2016).

CortexID spatially normalizes each PET examination to a template

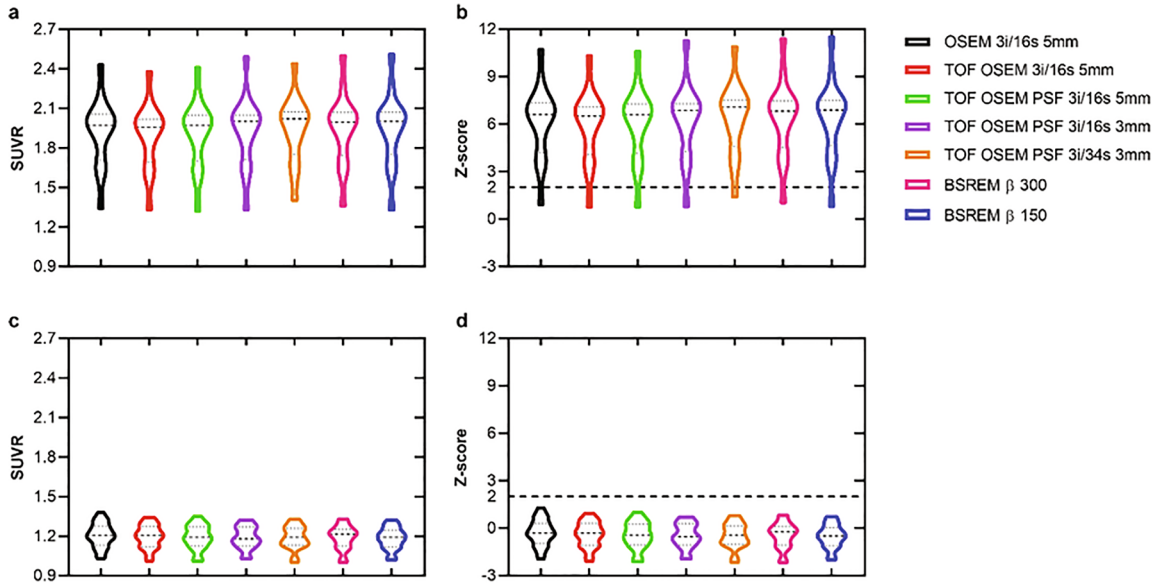

Fig. 3. SUVR and z-score derived from [^{18}F]flutemetamol PET image data of the composite region with cerebellar gray matter as reference. The graphs display patients (a,b) and healthy controls (c,d), and from left to right in each graph are OSEM, TOF OSEM, TOF OSEM PSF (three variants) and BSREM (two variants).

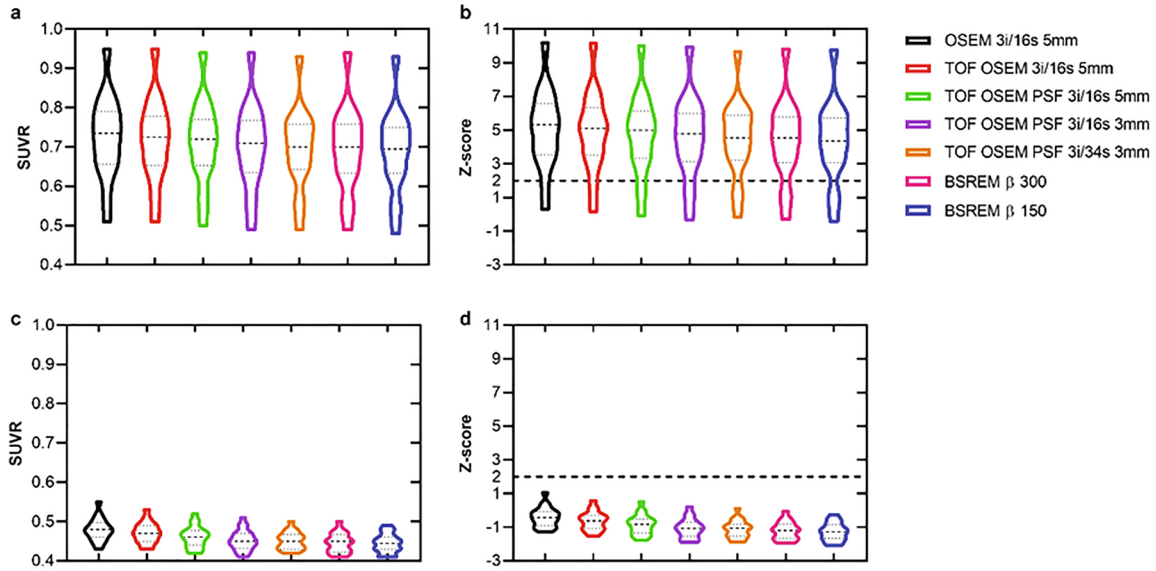

Fig. 4. SUVR and z-score derived from [^{18}F]flutemetamol PET image data of the composite region with pons as reference. The graphs display patients (a,b) and healthy controls (c,d), and from left to right in each graph are OSEM, TOF OSEM, TOF OSEM PSF (three variants) and BSREM (two variants).

space to account for anatomical variations. This normalization will differ slightly each time an examination is uploaded to the software and therefore this step may induce some variations to the outcome measures of the present study.

Cohen's d as a measure of effect size between patients and controls was found to be similar regardless if improved reconstructions methods were used and compared to each other. This suggests that it may not be beneficial to update existing normal databases to improve the outcome of software-aided diagnosis systems. However, on the basis of our study, employing image reconstruction methods other than those used for acquisition of the normal database may negatively affect the clinical assessment outcome. Hence, two image reconstructions may be required to benefit from the new developments in PET instrumentation and software design; one that is similar to the database of the software-aided diagnosis system for quantitative assessment and another employing improved image reconstruction methods for visual assessment.

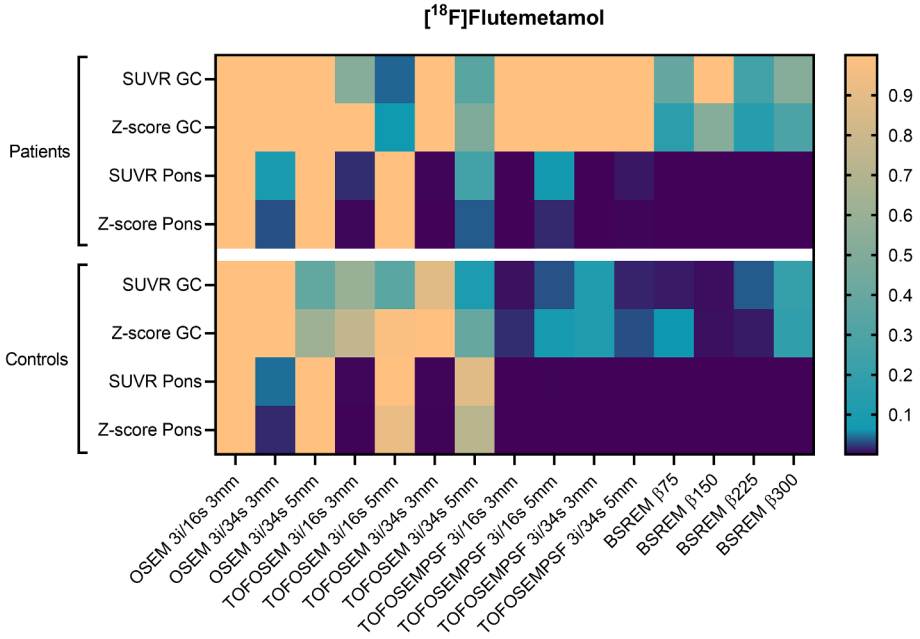

Fig. 5. Adjusted P-values from nonparametric Friedman test correcting for multiple comparisons using Dunn's statistical hypothesis testing. Family wise significance at 0.05. All reconstructions are compared to OSEM 3i/16s 5 mm filter with the same reference region. GC: gray cerebellum.

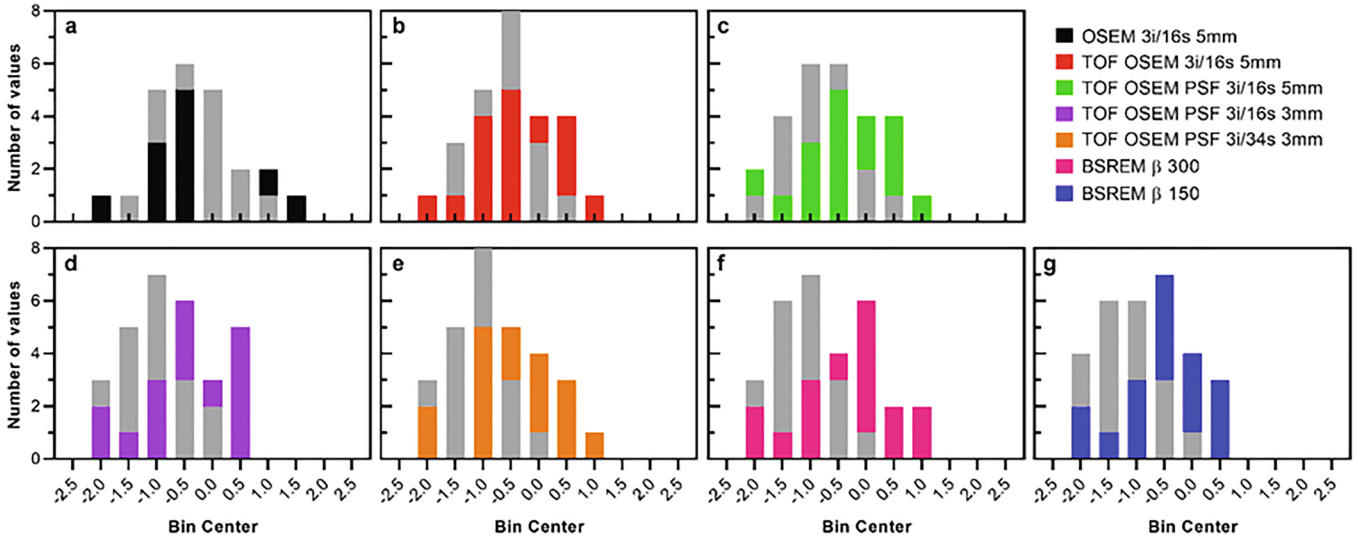

Fig. 6. Z-score histograms derived from [^{18}F]flutemetamol healthy control PET image data of the composite region. Cerebellar gray matter (bars in color) and pons (bars in gray) were used as reference regions.

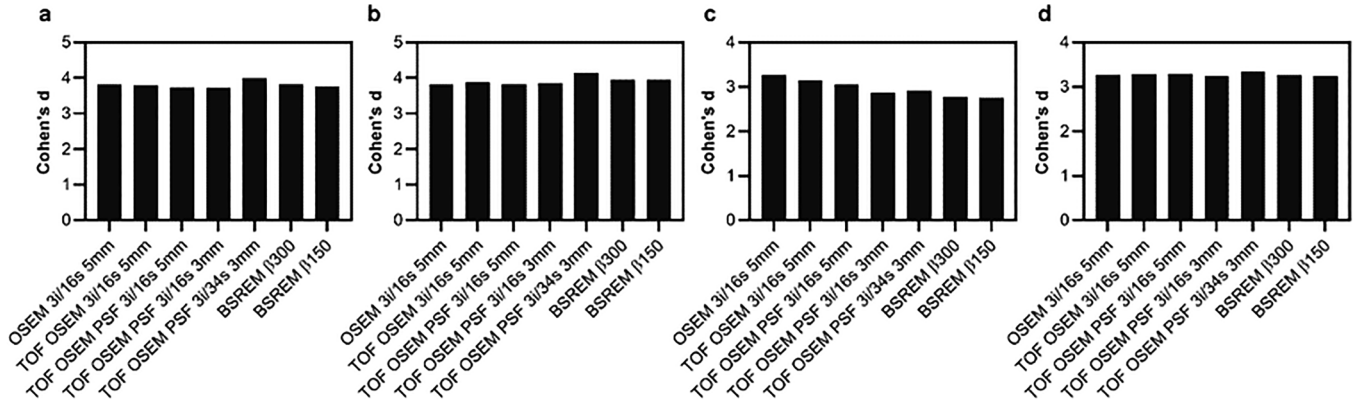

Fig. 7. Cohen's d derived from SUVR [^{18}F]flutemetamol PET image data of the composite region. Patients compared to controls (controls reconstructed using OSEM 3i/16 s 5 mm (a,c) or same reconstruction as patients (b,d)). Cerebellar gray matter (a,b) and pons (c,d) were used as reference regions.

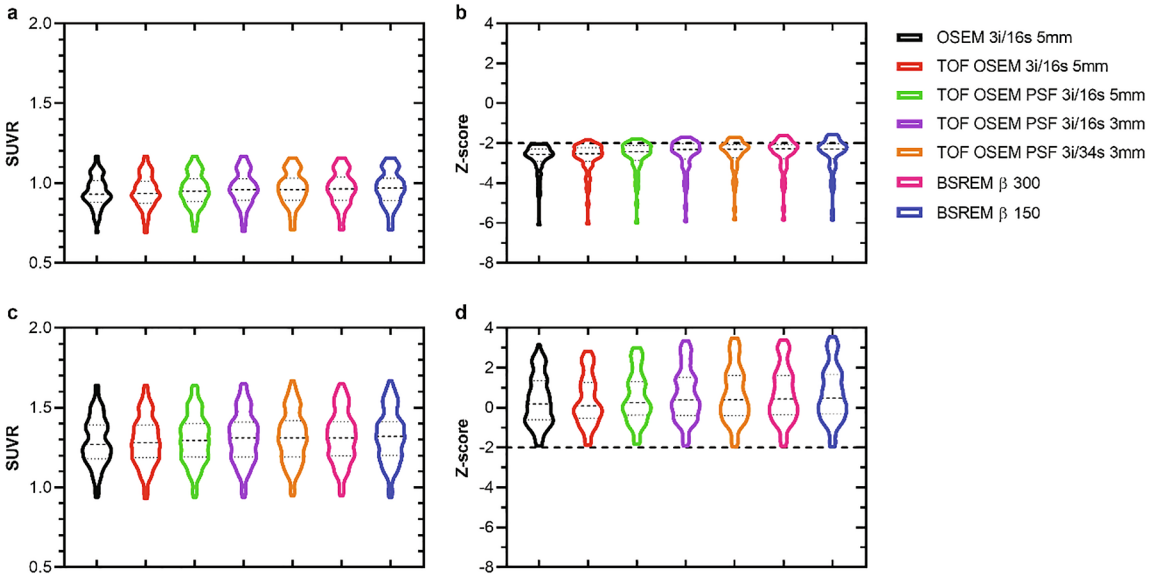

Fig. 8. SUVR and z-score derived from [^{18}F]FDG PET image data of the prefrontal, precuneus and parietal region with whole cerebellum as reference. The graphs display patients (a,b) and healthy controls (c,d), and from left to right in each graph are OSEM, TOF OSEM, TOF OSEM PSF (three variants) and BSREM (two variants).

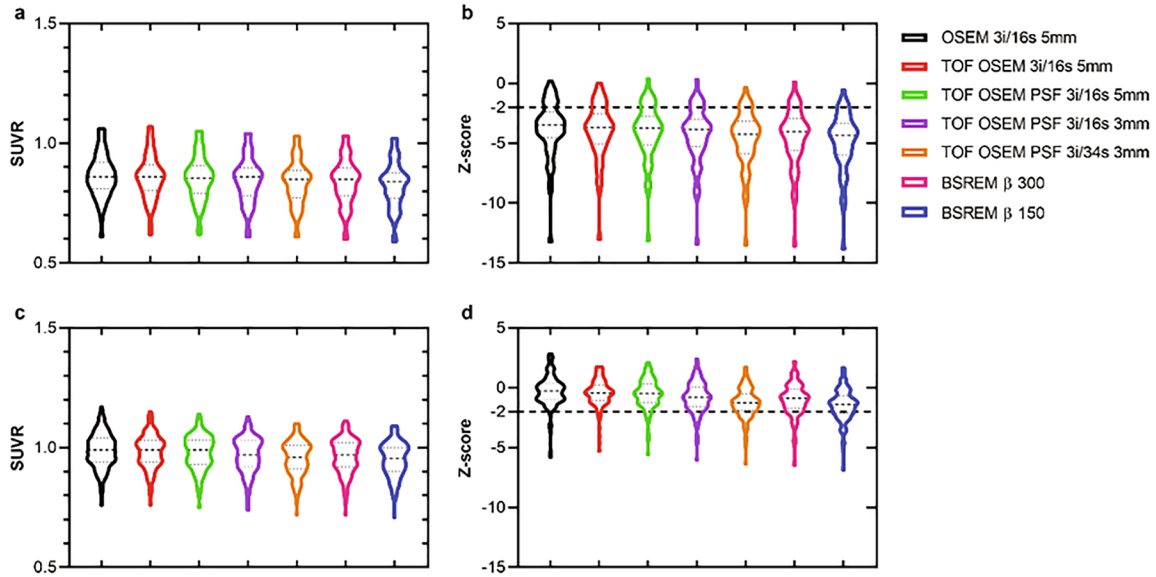

Fig. 9. SUVR and z-score derived from [^{18}F]FDG PET image data of the prefrontal, precuneus and parietal region with whole brain as reference. The graphs display patients (a,b) and healthy controls (c,d), and from left to right in each graph are OSEM, TOF OSEM, TOF OSEM PSF (three variants) and BSREM (two variants).

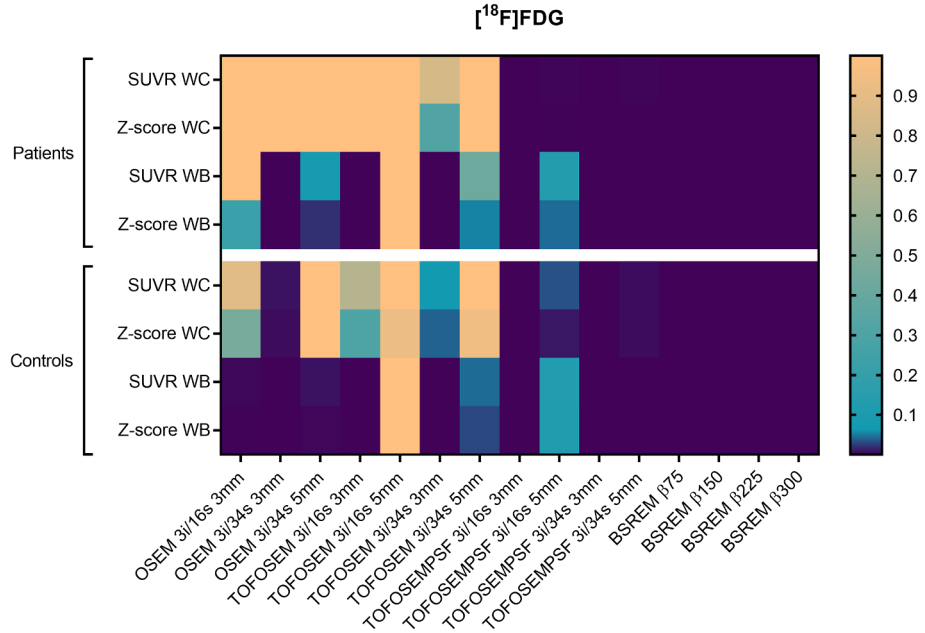

Fig. 10. Adjusted P-values from nonparametric Friedman test correcting for multiple comparisons using Dunn's statistical hypothesis testing. Family wise significance at 0.05. All reconstructions are compared to OSEM 3i/16s 5 mm filter with the same reference region. WC: whole cerebellum; WB: whole brain.

5. Conclusions

Software-aided assessment of patient pathologies was affected by image reconstruction methods and should be used with caution when employing other image reconstruction methods than those used for acquisition of the normal database. The selection of reference region influenced the outcome measures and increased absolute differences between reconstructions methods, therefore cerebellar gray matter and whole cerebellum should be used as reference region for [^{18}F]flutemetamol and [^{18}F]FDG, respectively, and use of pons and whole brain should be avoided.

Author contributions

All authors contributed to the study design. Jenny Oddstig, Oskar Hansson and Elin Lindström collected the data. Elin Lindström performed the data analysis and prepared the first draft of the manuscript. All authors revised the manuscript drafts as well as read and approved the final manuscript.

Conflicts of interest

A research agreement between Uppsala University Hospital and GE Healthcare partly supported this study (P.I. ML), covering the salary for EL. OH has acquired research support (for the institution) from Roche, Pfizer, GE Healthcare, Biogen, AVID Radiopharmaceuticals and Euroimmun. In the past 2 years, he has received consultancy/speaker fees (paid to the institution) from Biogen and Roche. The other authors declare that they have no conflict of interest.

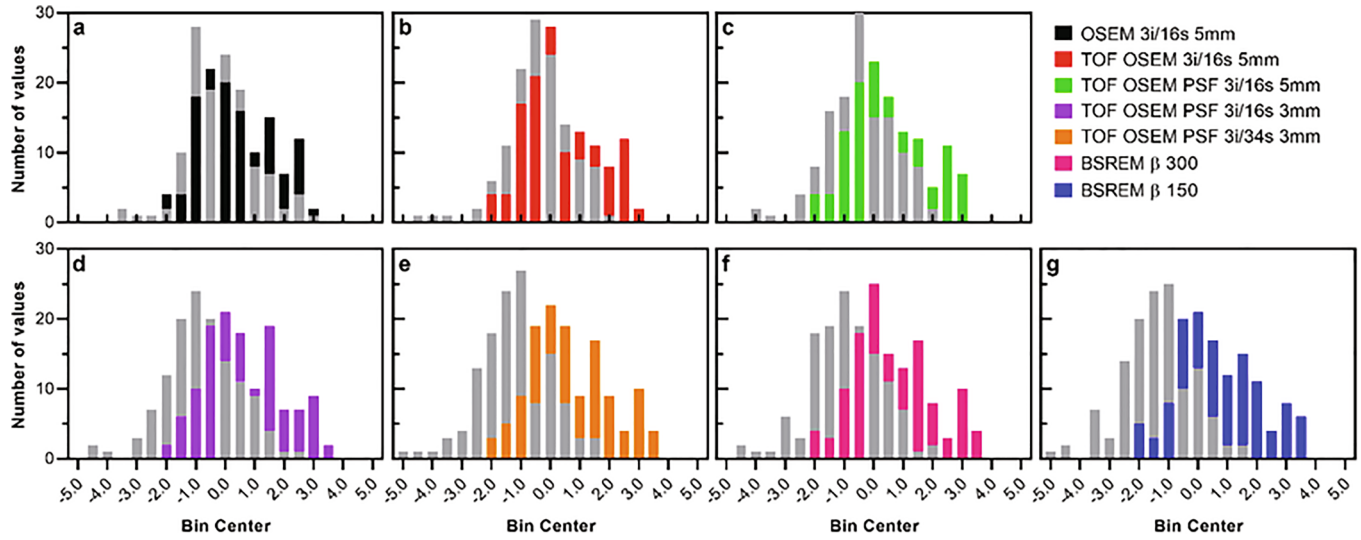

Fig. 11. Z-score histograms derived from [^{18}F]FDG healthy control PET image data of the prefrontal, precuneus and parietal regions. Whole cerebellum (bars in color) and whole brain (bars in gray) were used as reference regions.

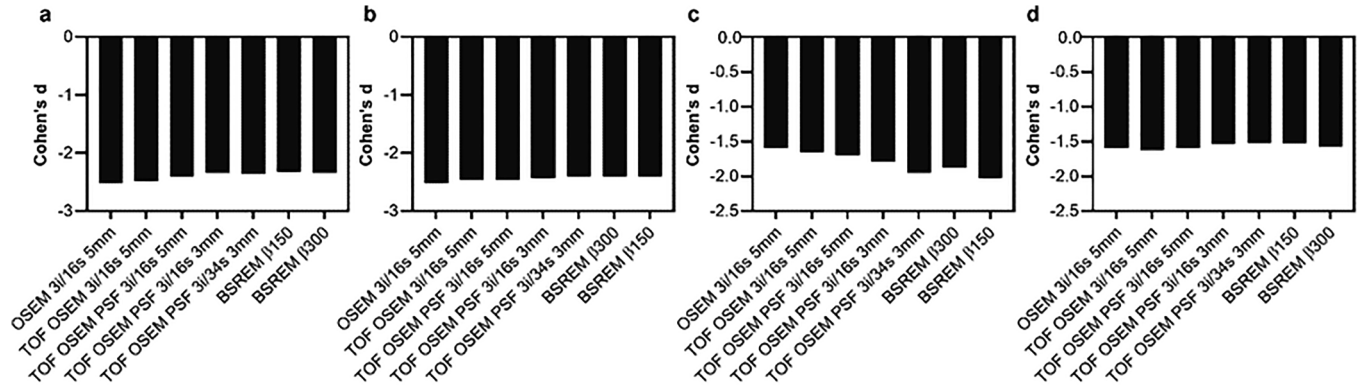

Fig. 12. Cohen's d derived from SUVR [^{18}F]FDG PET image data of the prefrontal, precuneus and parietal regions. Patients compared to controls (controls reconstructed using OSEM 3i/16s 5 mm (a,c) or same reconstruction as patients (b,d)). Whole cerebellum (a,b) and whole brain (c,d) were used as reference regions.

CRediT authorship contribution statement

Elin Lindström: Conceptualization, Methodology, Formal analysis, Data curation, Writing - original draft, Writing - review & editing. **Jenny Oddstig:** Resources, Writing - review & editing. **Torsten Danfors:** Resources, Writing - review & editing. **Jonas Jögi:** Resources, Writing - review & editing. **Oskar Hansson:** Resources, Writing - review & editing, Funding acquisition. **Mark Lubberink:** Conceptualization, Writing - review & editing, Project administration, Funding acquisition.

Acknowledgments

We would like to acknowledge the staff at the Uppsala University Hospital PET-Centre for performing examinations. Furthermore, Jens Sörensen and Anders Sundin are greatly appreciated for discussions and for providing valuable inputs.

Funding

This study was financed by a research grant from GE Healthcare and the Swedish government under the ALF agreement. The BioFINDER 2 study was supported by the Swedish Research Council, the Knut and Alice Wallenberg foundation, the Marianne and Marcus Wallenberg foundation, the Swedish Alzheimer Foundation, the Swedish Brain Foundation, the Skåne University Hospital Foundation, and the Swedish government under the ALF agreement.

Ethics approval

All procedures performed in this study were in accordance with the ethical standards of the institutional research committee (approvals from the regional ethical authority of each participating cite: Malmö/Lund reference number 2016/1053 and Uppsala reference number 2019/00092) and with the 1964 Helsinki declaration and its later amendments or comparable ethical standards.

Data availability

The datasets generated during and/or analyzed during the current study are available from the corresponding author on reasonable request.

Appendix A. Supplementary data

Supplementary data to this article can be found online at https://doi.org/10.1016/j.nicl.2020.102386.

References

Björsdorff, M., Oddstig, J., Karindotter-Borgendahl, N., Almquist, H., Zackrisson, S., Minark, D., et al., 2019. Impact of penalizing factor in a block-sequential regularized expectation maximization reconstruction algorithm for 18F-fluorcholine PET-CT regarding image quality and interpretation. EJNMMI Phys. 6, 5.

De Pierro, A.R., Yamagishi, M.E.B., 2001. Fast EM-like methods for maximum 'a posteriori' estimates in emission tomography. IEEE Trans. Med. Imaging. 20, 280–288.

Drzezga, A., 2009. Diagnosis of Alzheimer's disease with [18F]PET in mild and asymptomatic stages. Behav. Neurol. 21, 101–115.

Finnsson, J., Lubberink, M., Savitcheva, I., Fällmar, D., Melberg, A., Kumlien, E., et al., 2019. Glucose metabolism in the brain in LMNB1-related autosomal dominant leukodystrophy. Acta. Neurol. Scand. 139, 135–142.

Fällmar, D., Lilja, J., Kilander, L., Danfors, T., Lubberink, M., Larsson, E.M., et al., 2016. Validation of true low-dose (18)F-FDG PET of the brain. Am. J. Nucl. Med. Mol. Imaging. 6, 269–276.

Hsu, D.F.C., Ilan, E., Peterson, W.T., Uribe, J., Lubberink, M., Levin, C.S., 2017. Studies of a next generation silicon-photomultiplier-based time-of-flight PET/CT system. J. Nucl. Med. 58, 1511–1518.

Ishii, K., Kono, A.K., Sasaki, H., Miyamoto, N., Fukuda, T., Sakamoto, et al., 2006. Fully automatic diagnostic system for early- and late-onset mild Alzheimer's disease using FDG PET and 3D-SSP. Eur. J. Nucl. Med. Mol. Imaging. 33, 575–583.

Janelidze, S., Pannee, J., Mikulskis, A., Chiao, P., Zetterberg, H., Blennow, K., et al., 2017. Concordance between different amyloid immunoassays and visual amyloid positron emission tomographic assessment. JAMA Neurol. 74, 1492–1501.

Josephs, K.A., Duffy, J.R., Strand, E.A., Machulda, M.M., Senjem, M.L., Master, A.V., et al., 2012. Characterizing a neurodegenerative syndrome: primary progressive apraxia of speech. Brain. 135, 1522–1536.

Joshi, A.D., Pontecorvo, M.J., Lu, M., Skovronsky, D.M., Mintun, M.A., Devous Sr, M.D., 2015. A semiautomated method for quantification of 18F-florbetapir PET images. J. Nucl. Med. 56, 1736–1741.

Lindström, E., Sundin, A., Trampal, C., Lindsjö, L., Ilan, E., Danfors, T., et al., 2018. Evaluation of penalized-likelihood estimation reconstruction on a digital time-of-flight PET/CT scanner for 18F-FDG whole-body examinations. J. Nucl. Med. 59, 1152–1158.

Lindström, E., Velikyan, I., Regula, N.K., Alhuseinalkhudhur, A., Sundin, A., Sörensen, J., et al., 2019. Regularized reconstruction of digital time-of-flight 68Ga-PSMA-11 PET/CT for the detection of recurrent disease in prostate cancer patients. Theranostics. 9, 3476–3484.

Lindström, E., Lindsjö, L., Sundin, A., Sörensen, J., Lubberink, M., 2020. Evaluation of block-sequential regularized expectation maximization reconstruction of 68Ga-DOTATOC, 18F-fluoride, and 11C-acetate whole-body examinations acquired on a digital time-of-flight PET/CT scanner. EJNMMI Phys. 7.

Minoshima, S., Frey, K.A., Koeppe, R.A., Foster, N.L., Kuhl, D.E., 1995. A diagnostic approach in Alzheimer's disease using three-dimensional stereotactic surface projections of fluorine-18-FDG PET. J. Nucl. Med. 36, 1238–1248.

Mosconi, L., Tsui, W.H., Herholz, K., Pupi, A., Drzezga, A., Lucignani, G., et al., 2008. Multicenter standardized 18F-FDG PET diagnosis of mild cognitive impairment, Alzheimer's disease, and other dementias. J. Nucl. Med. 49, 390–398.

Nuyts, J., Bequé, D., Dupont, P., Mortelmans, L., 2002. A concave prior penalizing relative differences for maximum-a-posteriori reconstruction in emission tomography. IEEE Trans. Nucl. Sci. 49, 56–60.

Partovi, S., Yuh, R., Pirozzi, S., Lu, Z., Couturier, S., Grosse, U., et al., 2017. Diagnostic performance of an automated analysis software for the diagnosis of Alzheimer's dementia with ^{18}F FDG PET. AM. J. Nucl. Med. Mol. Imaging. 7, 12–23.

Ross, S.Q., 2014. Clear White Paper. GE Healthcare, Chicago, IL.

Sah, B.R., Stolzmann, P., Delso, G., Wollenweber, S.D., Hüllner, M., Hakami, Y.A., et al., 2017. Clinical evaluation of a block sequential regularized expectation maximization reconstruction algorithm in 18F-FDG PET/CT studies. Nucl. Med. Commun. 38, 57–66.

Teoh, E.J., McGowan, D.R., Bradley, K.M., Belcher, E., Black, E., Gleason, F.V., 2016. Novel penalised likelihood reconstruction of PET in the assessment of histologically verified small pulmonary nodules. Eur. Radiol. 26, 576–584.

Thurfjell, L., Lilja, J., Lundqvist, R., Buckley, C., Smith, A., Vandenberghe, R., et al., 2014. Automated quantification of 18F-flutemetamol PET activity for categorizing scans as negative or positive for brain amyloid: concordance with visual image reads. J. Nucl. Med. 55, 1623–1628.

Trägårdh, E., Minarik, D., Almquist, H., Bitzén, U., Garpered, S., Hvittfelt, E., et al., 2019. Impact of acquisition time and penalizing factor in a block-sequential regularized expectation maximization reconstruction algorithm on a Si-photomultiplier-based PET-CT system for 18F-FDG. EJNMMI Res. 9, 64.